

RSC Advances



This is an *Accepted Manuscript*, which has been through the Royal Society of Chemistry peer review process and has been accepted for publication.

Accepted Manuscripts are published online shortly after acceptance, before technical editing, formatting and proof reading. Using this free service, authors can make their results available to the community, in citable form, before we publish the edited article. This *Accepted Manuscript* will be replaced by the edited, formatted and paginated article as soon as this is available.

You can find more information about *Accepted Manuscripts* in the [Information for Authors](#).

Please note that technical editing may introduce minor changes to the text and/or graphics, which may alter content. The journal's standard [Terms & Conditions](#) and the [Ethical guidelines](#) still apply. In no event shall the Royal Society of Chemistry be held responsible for any errors or omissions in this *Accepted Manuscript* or any consequences arising from the use of any information it contains.



One-Step Process of Nickel-based/Carbon Nanofoam Composite Supercapacitor Electrode Using Na_2SO_4 as Eco-friendly Electrolyte

R. Della Noce^{a*}, S. Eugénio^a, M. Boudard^b, L. Rapenne^b, T.M. Silva^{ac}, M.J. Carmezim^{ad}, S.W. Donne^e, and M.F. Montemor^a

Received 00th January 20xx,
Accepted 00th January 20xx

DOI: 10.1039/x0xx00000x

www.rsc.org/

In this work, NiO_x is anodically electrodeposited onto carbon nanofoam (CNF) to form a composite electrode devoted to supercapacitor applications. The use of NiSO_4 as precursor in electrodeposition results in the formation of NiO and NiOOH species, as confirmed by XPS analysis, by means of an one-step anodic process. The presence of both NiO and NiOOH suggests the existence of pseudocapacitance as observed in MnO_2 and RuO_2 materials. By employing Na_2SO_4 , an eco-friendly electrolyte, the resulting composite delivers a specific capacitance of 150 F g^{-1} at 1 A g^{-1} considering the total mass of the electrode (deposit plus substrate). In addition, this composite electrode can operate in a very broad potential window, as high as 2.2 V, suggesting its application in high energy density electrochemical supercapacitors

1. Introduction

Currently, electrochemical energy storage devices (EESD) combining high energy and high power densities are at the forefront of research. Among these, supercapacitors (SCs) play a major role because they can deliver much higher power than batteries. In this sense, SCs display considerable advantages compared to other EESDs such as high power capability, excellent reversibility (charge efficiency >95%), and long cycle life (> 10^5 cycles). In general, they exhibit 20–200 times larger capacitance per unit volume or mass than conventional electrolytic capacitors. Therefore, a number of applications now use SCs or are strongly considering them, including electric/hybrid vehicles, digital communication devices, digital cameras, mobile phones,

uninterruptible power supplies, smart grids, and storage of energy generated by renewable sources.¹

Despite the advantages concerning the utilization of metallic oxides for electrodes in asymmetric supercapacitors, especially their high theoretical specific capacitance, they still present some shortcomings. Of them, low conductivity (except for RuO_2) and the possibility of volume variation during the charge-discharge process are of main concern. These characteristics usually lead to poor rate capability and long-term stability of the resulting electrode which limits its practical applications in supercapacitors.

Carbon-based materials have been largely employed as electrode materials for supercapacitors in different forms. Such forms include a wide variety of architectures such as carbon nanotubes, activated carbons, mesoporous carbons, graphene, carbon onions, templated carbons, carbide-derived carbons, carbon nanospheres, among others.² Although carbon-based electrodes exhibit outstanding cyclic stability, long lifetime, and high power density they usually suffer from low specific capacitance compared to that of metal oxides, which is generally no more than 200 F g^{-1} . As a consequence, when assembled in supercapacitors, these

^a Centro de Química Estrutural-CQE, Departament of Chemical Engineering, Instituto Superior Técnico, Universidade de Lisboa, 1049-001 Lisboa, Portugal. E-mail: rodrigo.noce@tecnico.ulisboa.pt

^b Univ. Grenoble Alpes, LMGP, F-38000 Grenoble & CNRS, LMGP, F-38000 Grenoble, France

^c Department of Mechanical Engineering, GI-MOSM, Instituto Superior de Engenharia de Lisboa, 1950-062 Lisboa, Portugal.

^d ESTSetúbal, Instituto Politécnico de Setúbal, 1959-007 Setúbal, Portugal.

^e Discipline of Chemistry, University of Newcastle, Callaghan, NSW 2308, Australia.

carbonaceous materials result in devices with relatively low energy density, normally no higher than 5 Wh kg^{-1} , which is considerably lower than that of batteries ($30\text{--}40 \text{ Wh kg}^{-1}$ for lead acid and $50\text{--}250 \text{ Wh kg}^{-1}$ for lithium-ion systems).³

One of the strategies recently developed to enhance energy density in SCs consists in combining carbon-based materials with metallic oxides to form a composite electrode. This electrode presents a better capacitive performance and overcomes the above-mentioned drawbacks for each individual component. In this context, considerable benefits can be achieved by this approach, i.e.,

1) Carbon not only acts as the physical support of metal oxides but also gives rise to channels for charge transport. Its high electronic conductivity enhances the rate capability and power density at large charge/discharge currents.

2) As metal oxides commonly possess one order of magnitude higher specific capacitance than carbon materials, they will significantly contribute to increase the energy density of the resulting material electrode since the latter is directly proportional to the material capacitance.

3) In general, carbon-based materials can be more cost-effective than metal oxides, in particular those synthesized from natural precursors namely activated carbons, which can result in cost reduction of the final product.⁴

All of these characteristics envisage the development of supercapacitors electrodes that can exhibit at the same time high power and energy densities as well as good rate capability and cyclic stability. These four parameters are extremely important to the production of high performance supercapacitors.

Ni-based materials, mainly Ni(OH)_2 have been studied as supercapacitor electrodes in several reports,⁵⁻⁷ in which they are referred as pseudocapacitive materials. However, this concept is controversial and has been discussed by authors such as Brousse et al.⁸ This author proposes that an electrode material exhibiting pseudocapacitive behavior must display a linear dependence of the charge stored with changing potential within the working window. This is clearly observed in materials such as MnO_2 , RuO_2 , and more recently Nb_2O_5 ,⁹ where their electrochemical signature; e.g., cyclic

voltammetry and charge-discharge curves, show rectangular- and triangular-like shaped forms, respectively, similar to those observed in activated carbon materials.

Apart from the electrode material, another important component of a supercapacitor device is its electrolyte. By employing appropriate electrolytes, the energy density in SCs can be increased considerably since this parameter is directly proportional to voltage squared (i.e., $E = CV^2/2$). In this sense, many efforts and funds have been spent on the development of new supercapacitor electrolytes mainly organic solvents and ionic liquids (ILs) that have a larger electrochemical stability window when compared to aqueous solutions. For instance, by using 2-methylpyridine and trifluoroacetic acid based IL as an electrolyte, the working potential window of RuO_2 could be extended up to 2.5 V delivering a specific capacitance of 83 F g^{-1} obtained at 5 mV s^{-1} .¹⁰ However, organic electrolytes and ILs present in general poor conductivity and high viscosity when compared to aqueous systems resulting in low capacitance values. Furthermore, most of them are quite expensive and environmentally-unfriendly. Therefore, aqueous electrolytes are still more advantageous from a cost and ecological viewpoint. In this context, KOH solutions have been utilized frequently as supercapacitor electrolyte in a variety of materials, especially in Ni- and Co-based charge storage electrodes. In general, KOH electrolytes give rise to higher values of specific capacitance when compared to other aqueous electrolytes such as Na_2SO_4 , due to the small size of both K^+ and OH^- ions which leads to a faster intercalation process. On the other hand, KOH is a corrosive solution particularly when used in high concentrations (up to 8 M), which limits its general use in commercial supercapacitors.

In this work, we report on the design of a NiO_x/CNF composite as supercapacitor electrode by using a one-step anodic electrodeposition process. It is demonstrated that by using Na_2SO_4 as the electrolyte, a neutral and environmentally friendly solution, the composite electrode can operate in a very broad potential window as high as 2.2 V. The resulting supercapacitor electrode delivers a specific capacitance of 150 F g^{-1} at 1 A g^{-1} considering the total mass of the electrode (deposit plus substrate). In addition, it is shown the simultaneous formation of Ni^{2+} and Ni^{3+} species, confirmed by XPS, during the electrodeposition process which

might lead to the existence of pseudocapacitance as evidenced in MnO₂ and RuO₂ materials.

2. Experimental

2.1. NiO_x Electrodeposition

NiO_x was electrodeposited onto CNF (geometrical area of 2 cm²) which served as a current collector to form a composite electrode. The CNF properties have been previously described elsewhere.¹¹ The deposits were obtained from a bath composed of 0.1 M NiSO₄ and 0.1 M Na₂SO₄. The bath pH was set to 6 by adding dilute NaOH. Analytical grade chemicals were used to prepare all solutions.

NiO_x deposits were galvanostatically obtained by using a Voltalab PGZ 100 potentiostat/galvanostat at room temperature. A three-electrode conventional cell was used for all electrochemical measurements. The applied current density was varied from 2 to 20 mA cm⁻² and the charge density was kept constant at 40 C cm⁻². No stirring was performed during the electrodeposition process.

The weight of the NiO_x deposits was directly measured using an electronic microbalance (Sartorius, model MC 5, d = 0.01/0.1 mg). The mass loading of the active material was measured in all cases by subtracting the substrate mass from the total weight. In general, the mass loading of the deposits ranged from 1 to 1.5 mg corresponding to about 10% in weight of the CNF mass.

2.2. XPS Analysis

The chemical composition and the corresponding oxidation states of the species present in the deposits were assessed by XPS analysis. The XPS spectra were acquired in constant analyzer energy (CAE) mode (30 eV), using an Al (non-monochromatic) anode. The accelerating voltage was 15 kV. The quantitative XPS analysis was performed using the Avantage[®] software. All spectra were referred to C 1s at 284.7 eV.

2.3. TEM Analysis

The structural details were studied by transmission electron microscopy (TEM, JEOL JEM-2010 microscope) operating at 200 KeV. Two samples preparation were used. Samples were prepared by scratching using a diamond tip. Both pristine CNF and NiO_x electrodeposited at 2 mA cm⁻² onto CNF (NiO_x/CNF) were used

and the resulting powder was collected directly on TEM grids in order to avoid structural transformations induced by sample thinning process. Alternatively simple ultrasonic vibrations of the samples was used to detach the deposits for preparing the specimen on TEM grids.

2.4. Electrochemical Characterization

The electrochemical performance of the composite electrodes was assessed by cyclic voltammetry (CV) and chronopotentiometry. A platinum plate (geometrical area of 6 cm²) and a saturated calomel electrode (SCE) were used as counter and reference electrodes, respectively. All the experiments were performed in freshly prepared 1 M Na₂SO₄ electrolyte at room temperature. Cyclic voltammetry was carried out by varying the scan rate from 2 to 20 mV s⁻¹. Chronopotentiometry (charge-discharge curves) was conducted in a potential range from -1.20 to 1.00 V applying a specific applied current of 1 A g⁻¹. Moreover, a long-term cycling test constituted of 2500 cycles was carried out to verify the supercapacitor electrode stability.

A two-electrode configuration cell was used to evaluate the capacitive properties of the prepared composites. In this condition, the NiO_x/CNF electrode (positive) was connected in parallel to pure CNF (negative) simulating an asymmetric SC. The two electrodes were separated with a 0.25 mm thin filter paper soaked in 1 M Na₂SO₄ solution. Both cyclic voltammetry and chronopotentiometry were used to study its electrochemical performance. Charge-discharge cyclic stability of asymmetric test cell was conducted under constant current density of 1 A g⁻¹ by performing 2500 cycles.

3. Results and Discussion

3.1. NiO_x deposition

Fig. 1 displays the potential vs. time (E vs. t) profiles for the galvanostatic electrodeposition of NiO_x onto CNF at different current densities. As expected, the potential increases with increasing current density. An applied current of 2 mA cm⁻² was chosen as the optimal condition for electrodeposition because, as will be shown later, higher current density values, result in electrodes with lower capacitances probably due to the formation of some irreversible species at higher potentials. In fact, NiO_x has been anodically electrodeposited in both potentiostatic and galvanostatic modes from different precursors.¹²⁻¹⁴ Even though the

anodic electrodeposition process has slower kinetics than the cathodic process, it is a very useful route since it allows the deposition of high oxidation state oxides as evidenced in the case of MnO_2 , PbO_2 , and Ti_2O_3 materials.¹⁵

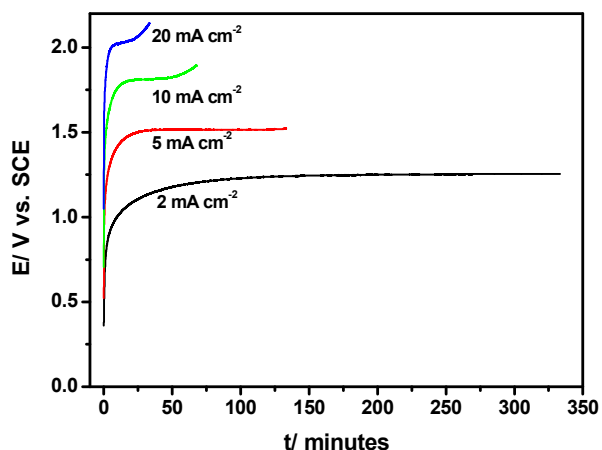


Figure 1. E-t profiles of the electrodeposition of NiO_x onto CNF obtained for different applied current densities.

In general, potential values between 0.9 and 1.5 V/SCE, or current densities ranging from 0.1 to 2 mA cm^{-2} lead to the formation of Ni oxides, hydroxides, and/or oxyhydroxides. For instance, Wu et al.¹³ reported the anodic deposition of thin NiO films (12-16 nm) from sulfate-based solutions on stainless steel by applying two different potentials (0.9 and 1.05 V/Ag/AgCl_{sat.}). After annealing at 300 °C for 1 h in air, NiO nanoflakes were obtained. Briggs and Fleischmann¹⁶ demonstrated the anodic deposition of pure NiOOH onto Pt from acetate solutions by applying constant potentials between 0.9 and 1.9 V/SCE. The current efficiency of the electrodeposition process decreases exponentially with increasing time. Furthermore, electrodeposition is also hindered as the applied potential increases due to higher oxygen evolution. For these reasons, it can be inferred that to obtain NiOOH deposits with reasonable thicknesses long deposition times are needed and an appropriate value of potential or current density must be selected in order to minimize the oxygen evolution side reaction.

3.2. TEM and XPS analyses

The NiO_x deposited onto CNF were submitted to different characterization techniques such as SEM, XRD, and Raman

spectroscopy. Nevertheless, due to the formation of very small NiO_x particles, none of these techniques provided a reasonable response. Hence, higher resolution techniques such as TEM and XPS were used to characterize the NiO_x deposits. When the pristine CNF and NiO_x/CNF were scratched to perform the samples, it was impossible to identify any NiOx particle and both examinations were identical revealing only the amorphous structure of the CNF as displayed in Fig. 2. However EDS (not shown) analysis on NiO_x/CNF clearly showed the presence of Ni, Na, S and O elements in addition to the C element present for the pristine CNF.

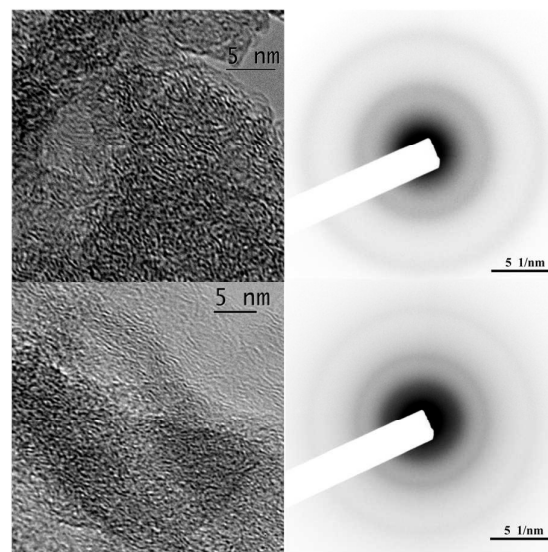


Figure 2. TEM results on pristine CNF (bottom) and NiO_x/CNF (top) for samples obtained by scratching.

The analysis on samples prepared by ultrasonic vibrations revealed the presence of different nanocrystals by high resolution TEM (HRTEM) imaging and by selected area electron diffraction (SAED). Fig. 3 shows the identification of relatively small nanocrystals of NiO (less than 10 nm in size) identified according to ICSD 9866 (Fm-3m (225) $a=4.178(1)$ Å) coexisting with larger nanocrystals of Na_2SO_4 nanocrystals, identified according to ICSD 63077 (P63/mmc (194) $a=5.326(2)$ Å $c=7.126(3)$ Å). The amount of NiO can vary from being almost unobservable, as in Fig. 3b where almost only Na_2SO_4 is observed, to a relatively abundant phase as in Fig. 3c. It was observed that in the region with initial no observable NiO in the SAED pattern its crystallization could be induced by in situ TEM beam heating which indicates that Ni can be in the form of badly crystallized compound as could be the case of oxyhydroxides. NiO always appears as homogeneous and broaden rings in the SAED

pattern corresponding to a random distribution of very small nanocrystals (less than 10 nm in size). It was also possible to observe the presence of relatively large crystals of Na_2SO_4 and (occasionally) NiSO_4 (submicronic to micronic in range). This clearly indicates that the electrolyte can be trapped in the CFN and then crystallize on drying.

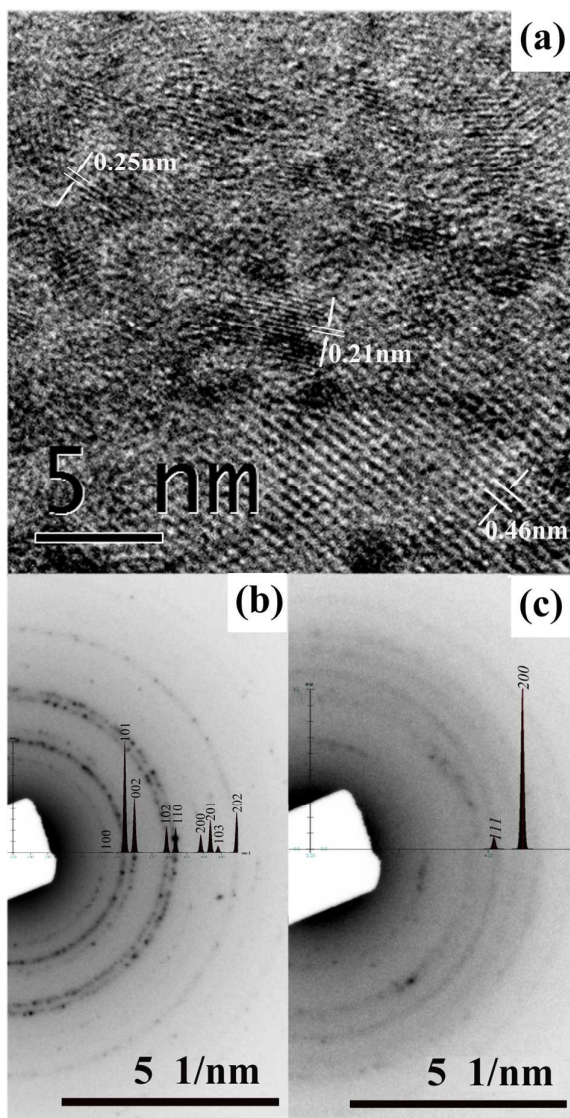
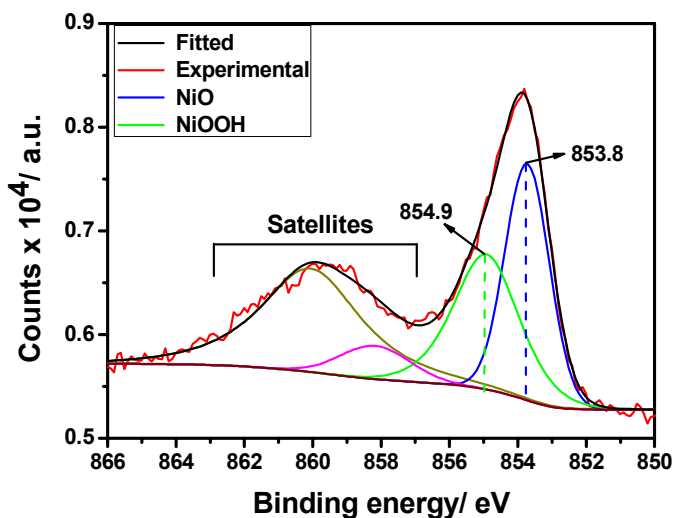


Figure 3. TEM results. (a) HRTEM images showing the presence of FCC NiO nanocrystals less than 10 nm in size (interplanar distances of 0.21 and 0.25 nm) coexisting with Na_2SO_4 nanocrystals of about 30 nm (interplanar distances of 0.46 nm). Indexation of SAED pattern of a region containing mainly Na_2SO_4 nanocrystals (b) and mixed Na_2SO_4 and NiO nanocrystals (c). Diffraction lines from the literature of Na_2SO_4 ¹⁷ (b) and NiO¹⁸ (c) are superimposed.

In order to better characterize the deposits, XPS was employed to assess the chemical composition and the corresponding

oxidation states of the species present in the deposits. Fig 2 depicts the high resolution photoelectron spectra for Ni $2p_{3/2}$ (a) and O 1s (b) elements taken for the NiO_x/CNF electrode prepared at 2 mA cm^{-2} . The Ni spectrum was deconvoluted into two main peaks at 853.8 and 854.9 eV which correspond to Ni^{2+} in NiO and Ni^{3+} in NiOOH, respectively. The $\text{Ni}^{2+}/\text{Ni}^{3+}$ ratio is equal to 3/2. Both species give rise to satellite peaks at higher binding energies as observed in Fig. 4a. The fact that NiOOH was not detected by previous TEM analysis can be due to its lower content and bad crystallization or amorphous character, as is often in the case for oxyhydroxides. With respect to the O spectrum, it was fitted by using three main peaks: the one at 533.5 eV is related to the presence of adsorbed water molecules.^{19,20} The other two peaks at 529.1 and 530.7 eV can be assigned to O^{2-} in NiO,²¹ and the typical metal-oxygen bonds of NiOOH,^{22,23} respectively. Recently, Gu et al.²⁴ has described the anodic electrodeposition of NiOOH film on passivated nickel foam for supercapacitors. Their XPS data have shown Ni and O peaks at 855.1 and 530.5 eV evidencing the formation of NiOOH species. Also, Dubé et al.²¹ has reported that NiO presents XPS peaks at 853.8 and 529.1 eV for Ni and O spectra, respectively. Hence, it can be said that our XPS results are in good agreement with those reported in the literature supporting the formation of both NiO and NiOOH species during the anodic electrodeposition process.



(a)

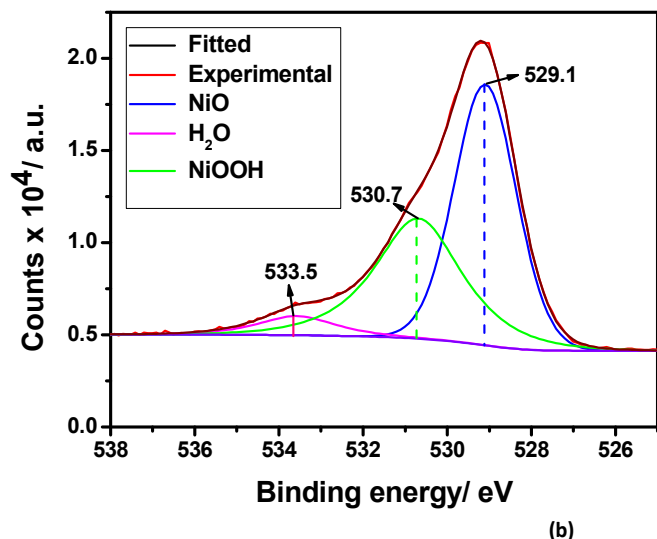
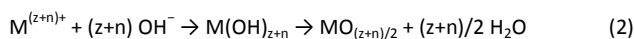


Figure 4. XPS spectra for (a) Ni ($2p_{3/2}$) and (b) O ($1s$) with their respective deconvolution. Spectra were taken for the NiO_x/CNF electrode prepared at 2 mA cm^{-2} .

The anodic electrodeposition process can be generally described by the following reactions¹⁵:



In this process, it is considered that the species with lower oxidation state is stable (Eq. 1) while the higher one undergoes hydrolysis to produce the metal oxide or hydroxide (Eq. 2). Then, it is a priori expected that in this final step only the formation of a species with higher oxidation state occurs, i.e. Ni^{2+} being converted to Ni^{3+} . However, in many anodic electrodeposition processes other species with different oxidation states can be concomitantly formed.²⁵⁻²⁷ For instance, Balasubramanian et al.²⁶ has reported the anodic electrodeposition synthesis of NiOOH films onto graphite by applying a constant potential of 1.10 V/SCE from a sulfate-containing bath. They have observed that the resulting deposits contain not only Ni^{3+} but also Ni^{2+} and Ni^{4+} species as evidenced by synchrotron X-ray absorption spectroscopy (XAS). Hu and Hsu²⁷ deposited $\text{CoO}_x \cdot n\text{H}_2\text{O}$ films onto graphite at a constant current density from chloride-based electrolytes with different complexing agents (acetate, citrate and EDTA). Irrespective of the employed complexing agent the anodically deposited film is a mixture of $\text{Co}(\text{II})$

and $\text{Co}(\text{III})$ species, such as CoOOH , $\text{Co}(\text{OH})_2$, and Co_3O_4 . It can be concluded that the anodic electrodeposition process is then governed by several parameters such as electrolyte composition and pH, applied potential/current density and deposition time, which may lead to the formation of deposits with different compositions with more than one oxidation state.

3.3. Electrochemical Tests

3.3.1. CNF in $1 \text{ M Na}_2\text{SO}_4$

Fig. 5a displays the cyclic voltammograms (CVs) for CNF in $1 \text{ M Na}_2\text{SO}_4$ obtained at different scan rates. As expected, the CVs present a nearly rectangular-like shape, typical of carbon-based materials, except at the extremes of potential where reactions related to the instability of the system are pronounced. Furthermore, the working potential window is considerable high (approximately 2.4 V) due to the fact that both hydrogen and oxygen evolution only take place at the extremes of potential. As in our previous work,¹¹ this behavior can be attributed to a hydrogen storage phenomenon that occurs in activated carbon as proposed by Béguin et al.²⁸ According to this model, hydrogen is adsorbed into the carbon pores retarding the H_2 evolution process and consequently expanding the operating potential window.

The charge-discharge curves for CNF are presented in Fig. 5b. A triangular-like shape can be noticed, characteristic of carbonaceous materials. Also in accordance with the CV results, the working potential window is significantly large (2.2 V) leading to a specific capacitance of 60 F g^{-1} at 1 A g^{-1} . Although this value is not as high as that previously obtained for CNF in 1 M KOH (130 F g^{-1}),¹¹ the potential window is 0.2 V higher. On the other hand, the CNF rate capability (insert of Fig. 5b) presents an improved performance in Na_2SO_4 . About 67% of the capacitance is retained when the current density is increased up to 3 A g^{-1} while only 56% retention was achieved when using KOH under the same conditions.¹¹ Additionally, it will be shown that by using Na_2SO_4 electrolyte improves the cyclability (capacitance retention) of the resulting composite.

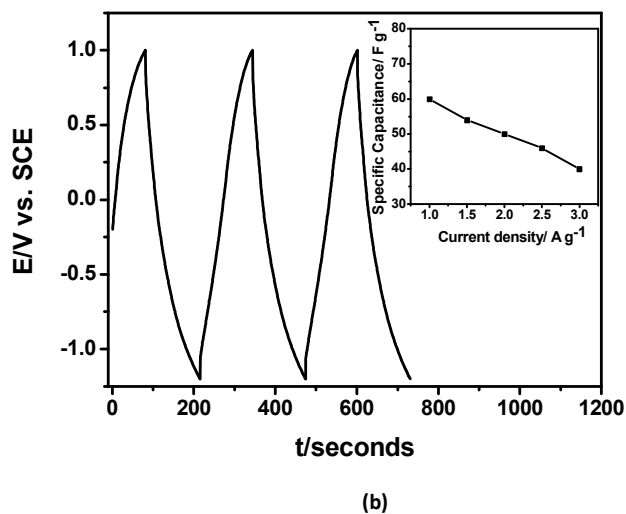
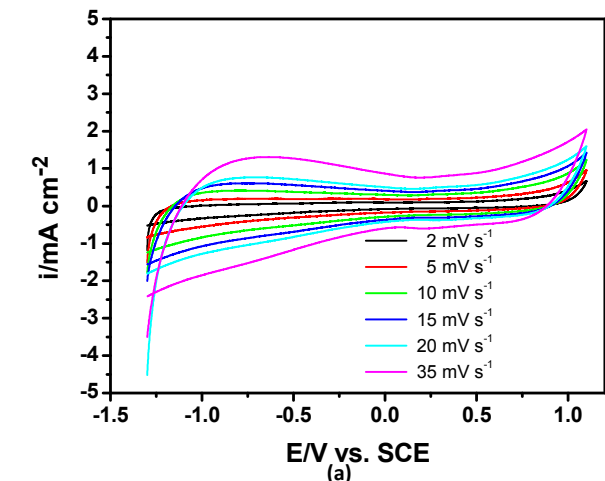


Figure 5. CVs obtained at different scan rates (a), charge-discharge curves at 1 A g^{-1} (b), and rate capability at different current densities (insert b) for CNF substrate in $1 \text{ M Na}_2\text{SO}_4$.

3.3.2. NiO_x/CNF cyclic voltammetry

Fig. 6a shows the CVs at different scan rates obtained for the NiO_x/CNF composite prepared at 2 mA cm^{-2} . The curves typically have a reasonably rectangular-like shape where no evident redox peaks are observed, except for the presence of some shoulders at higher scan rates. In order to have an idea about the NiO_x effect on the voltammetric behavior of the composite, CVs for the bare CNF and deposit are plotted in Fig. 6b. It is evident that the measured current density of the electrode increases when NiO_x is deposited onto CNF. The existence of two different Ni species (NiO and

NiOOH), as determined by XPS analysis, is responsible for this increase in current density, which in turn leads to increased capacitance as well. It is interesting to emphasize that in the literature, composite electrodes formed of Ni oxides/hydroxides coupled with carbonaceous materials only present, in general, one Ni electroactive species.^{29,30} In this condition, the CVs exhibit well-defined faradaic peaks due to Ni reactions, which indicates that the resulting hybrid material exhibits characteristics of both supercapacitor (carbon) and battery-like materials (NiO_x). In our case, the formation of two concomitant Ni species onto CNF leads to the existence of pseudocapacitance in a mechanism similar to what happens in MnO₂ and RuO₂ materials. For example, in the case of Mn, the redox reactions between the III and IV oxidation states are the responsible for the reported pseudocapacitance.

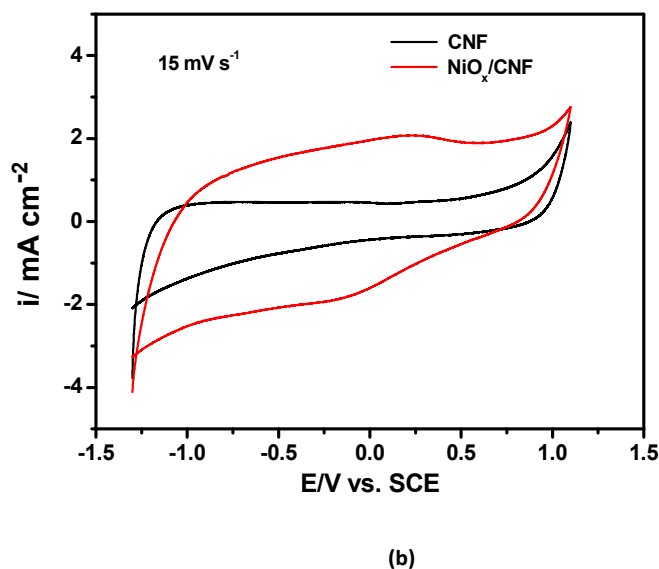
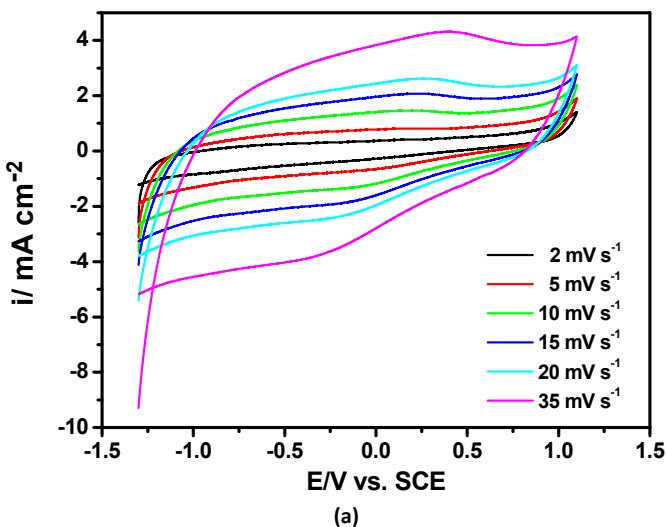
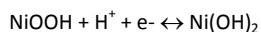


Figure 6. CVs at different scan rates obtained for the sample NiO_x/CNF prepared at 2 mA cm⁻² (a). CVs obtained at 15 mV s⁻¹ comparing the composite and bare CNF voltammetric behavior (b). Electrolyte: 1 M Na₂SO₄.

3.3.3. NiO_x/CNF chronopotentiometry (charge-discharge curves)

Knowing the limit potentials by CV, the charge-discharge curves for the NiO_x/CNF composite were studied. Fig. 7 illustrates the chronopotentiograms for the NiO_x/CNF composite prepared at 2 mA cm⁻². It is noticed that the composite electrode can operate in a potential window of 2.2 V and displays a triangular-like shape. The specific capacitance for the composite electrodes was calculated from these charge-discharge curves as described elsewhere,³¹ and are referred to the total mass loading of the substrate (CNF) plus the deposit (NiO_x). The specific capacitance of the composite is 150 F g⁻¹ at 1 A g⁻¹, which is 2.5 times higher than that of the bare CNF substrate. This value is similar to the work reported by Cheng et al.³² on demonstrating the formation of a supercapacitor composite electrode consisting of NiO deposited on carbon fiber paper scaffolds which delivers a specific capacitance of 84 F g⁻¹ (including the current collector) or 0.93 F cm⁻² at 1 mA cm⁻². However, the working potential window was limited to 0.8 V by using 2 M KOH as electrolyte. It is clear that the NiO_x species are responsible for the increase in capacitance of the NiO_x/CNF composite, which we have attributed to the pseudocapacitance originated by the presence of both NiO and NiOOH. In this sense, it is expected that our produced supercapacitor electrodes can work similarly to MnO₂ and RuO₂ materials,³³⁻³⁵ which exhibit the so-called pseudocapacitance mechanism. In the literature, Ni(OH)₂ and NiOOH are well known battery materials in an alkaline electrolyte, having featured in nickel-cadmium and nickel-metal hydride systems where their performance is excellent. To make the transition into a pseudocapacitive electrode system, where the redox processes they undergo contributes to the energy storage; i.e.,



the morphology of the nickel oxide materials has to be adapted and optimized to accommodate the anticipated high rate cycling of a pseudocapacitive material, as has been attempted in this work. This similarity in behavior between the nickel oxides and MnO₂ suggests that their pseudocapacitive behavior should also be similar.

The successful transition for a material from a battery material to a pseudocapacitive material is very dependent on its morphology, in particular the electrode-electrolyte interfacial area and crystallite size, and how they relate to the rate of electrochemical discharge. Fast discharge rates utilize fast redox processes on the electrode surface, such as double layer charge storage. Redox processes, and their contribution to the overall capacitance, depend on both the kinetics of charge transfer at the electrode-electrolyte interface, as well as solid state mass transfer of any intercalated species away from the interface into the bulk of the electrode material. Only with sufficiently fast kinetics and mass transport can the charge access the bulk structure, and thus provide an enhanced capacitance. Likewise, accessing the bulk structure has the potential to give rise to peaks in the voltammogram due to the reduction of specific sites within the solid state. Additionally, if the crystallite size of the electrode material is sufficiently small, and hence the diffusion lengths are relatively short, then an even more efficient utilization of the material structure will occur, as well as give rise to a voltammogram that is expected for a pseudocapacitive material; i.e., a box-like voltammogram.

With respect to the composite rate capability (the insert of Fig. 7), a decrease of specific capacitance with increasing the current density is observed. The NiO_x/CNF composite retains about 54% of its capacitance when the current density is increased from 1 to 3 A g⁻¹. This result is comparable to those reported in the literature for metal oxide/carbon composite materials. Zhang et al.³⁶ has reported that a composite formed of MnO₂ nanoparticles dispersed on hierarchical porous carbon (HPC) with a 0.52 mass ratio of MnO₂ to HPC-MnO₂ retains about 64% of its capacitance by increasing the current density from 1 to 3 A g⁻¹. In fact, this approach of coupling metal oxides with carbonaceous materials has been described as an effective way in the field of supercapacitors to circumvent the poor rate capability of metal oxides owing to their low electronic conductivity.⁴

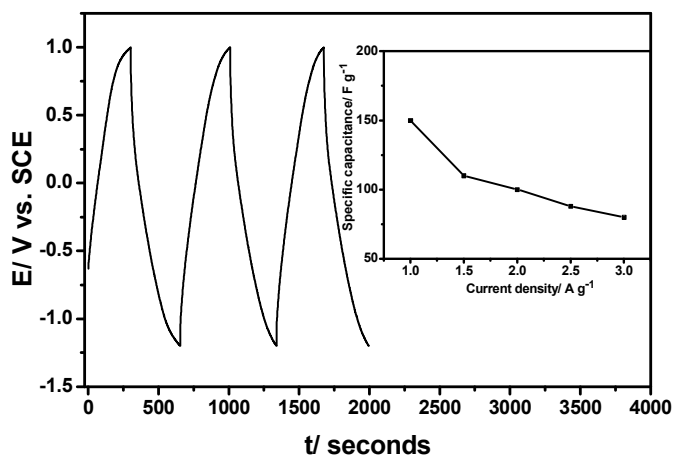


Figure 7. Charge-discharge curves at 1 A g^{-1} and rate capability at different current densities (insert) for NiO_x/CNF composite electrode prepared at 2 mA cm^{-2} in $1 \text{ M Na}_2\text{SO}_4$.

As mentioned above, the specific capacitance decreases with increasing applied current density for the anodic electrodeposition of NiO_x onto CNF (Fig. 8). This fact is most likely due to the formation of Ni irreversible species with electrodeposition at higher current densities, which may hinder the intercalation-deintercalation processes during charge-discharge, leading to a poor performance in terms of capacitance. Indeed, Silverman³⁷ updated the Pourbaix diagram for the nickel-water system and proposed the existence of two forms of $\text{Ni}(\text{OH})_2$, α and β . In alkaline solutions, the α form may revert to the β one. The author also proposed that NiOOH starts forming at approximately 1.4 V/SHE in neutral pH decreasing to 1.0 V when the pH is increased up to 10. By means of XRD and electron microscopy, it has been suggested that $\beta\text{-NiOOH}$ and $\gamma\text{-NiOOH}$ form in alkaline solutions. The Ni_3O_4 and $\text{Ni}_3\text{O}_4 \cdot 2\text{H}_2\text{O}$ species, proposed in the original diagram, do not seem to exist as compounds as suggested by the author. Most likely $\beta\text{-NiOOH}$ contains nickel in the +3 state only while $\gamma\text{-NiOOH}$ has been suggested to contain some nickel in a +4 state. The γ form may be converted to β upon aging.

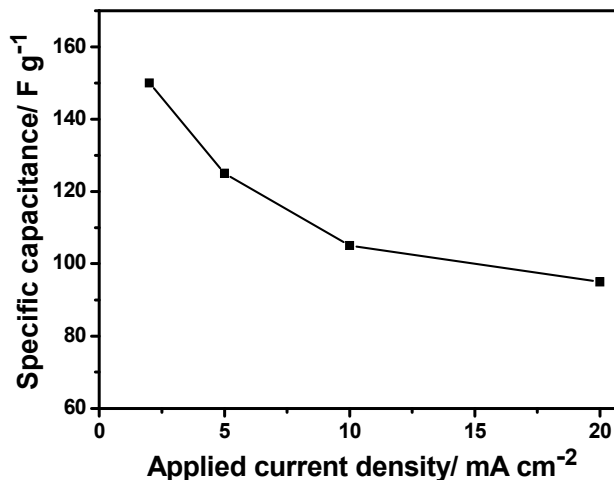


Figure 8. Variation of specific capacitance with applied current density for the anodic electrodeposition of NiO , onto CNF. Charge density: 40 C cm^{-2}

In order to verify the cyclability of the produced NiO_x/CNF composite, a long-term test, consisting of 2500 cycles at 1 A g^{-1} , was performed. Fig. 9 shows the capacitance retention as a function of cycle number for the NiO_x/CNF composite prepared at 2 mA cm^{-2} . It is noticed that the composite electrode retains 88.5% of its initial capacitance after 2500 cycles. In our previous work,¹¹ dealing with $\text{Co}(\text{OH})_2/\text{CNF}$ composite in 1 M KOH , a capacitance retention of 84% after 1000 cycles was verified in a working potential window of 2 V . Therefore, it can be concluded that the use of Na_2SO_4 as an electrolyte improves the electrode capacitance retention as expected since KOH is a more corrosive solution.

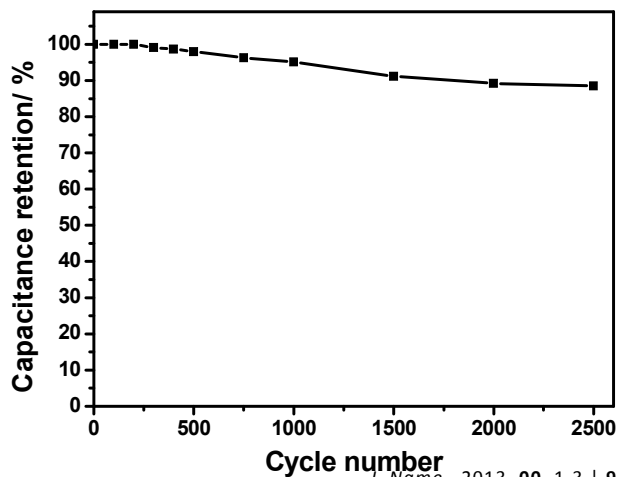


Figure 9. Capacitance retention as a function of cycle number for the NiO_x/CNF composite at 1 A g⁻¹ in 1 M Na₂SO₄.

3.3.4. Two-electrode set-up test

In order to test the capacitive performance of the prepared composites, a two-electrode set-up using the NiO_x/CNF composite, with NiO_x prepared at 2 mA cm⁻², as positive electrode and the pure CNF as negative electrode, was assembled. By doing so, it was possible to estimate the energy and power density of the cell simulating an asymmetric SC. However, the charge between positive and negative electrodes must be balanced in this case according to the following equation:

$$\frac{m_+}{m_-} = \frac{C_- \Delta E_-}{C_+ \Delta E_+} \quad (3)$$

Being *m*, *C* and ΔE the electrode mass, specific capacitance, and the potential window in the charge/discharge process for each individual electrode, respectively. Before measuring the charge-discharge curves for the cell, CV was performed to better visualize the working potential window (Fig. 10). It is noticed a rectangular-like shape of the CVs in all studied scan rates. The potential was swept up to 1.8 V where it is possible to observe the beginning of the oxygen evolution reaction related to an increase in current. For this reason, it was decided that 1.7 V is the limit for the operating potential window of the cell.

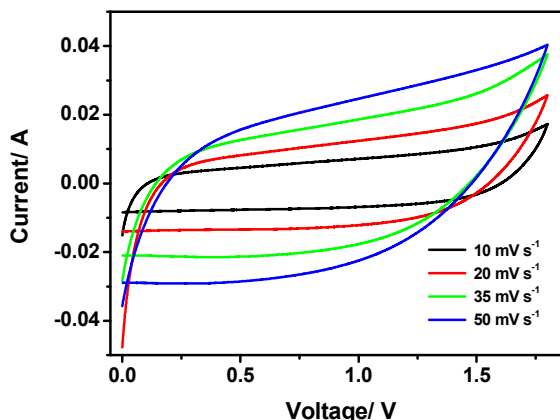


Figure 10. CV of NiO_x/CNF-CNF cell at different scan rates in 1 M Na₂SO₄.

Knowing the limit potential that the cell can operate, the charge-discharge curves were performed at 1 A g⁻¹ in 1 M Na₂SO₄ solution. Fig. 11a shows the charge-discharge curve for the NiO_x/CNF-CNF cell. By calculating the cell specific capacitance, it was found a value of 21.8 F g⁻¹. Thus, the energy density value ($E = CV^2/2$) was estimated which is 29 Wh kg⁻¹. In order to calculate the power density, the following expression was used:

$$P = \frac{1}{4} \frac{V^2}{R} \quad (4)$$

Where *V* is the cell potential window, 1.7 V in this case, and *R* is the internal resistance which can be related to the ohmic drop observed in the charge-discharge curve of the proposed cell. By extracting the ohmic drop from the curve in Fig. 11a (0.15V), *R* is 2.5 Ω. Knowing the *R* value, the power density is calculated which is 4 kW kg⁻¹.

The stability of the proposed cell was analyzed by a long term cycling test which consisted of 2500 cycles. Fig. 11b illustrates the variation of specific capacitance of the cell as a function of cycle numbers. It is noticed that the cell retains 85 % of its capacitance after 2500 cycles. In summary, the current results suggest the potential application of our produced composite electrodes in high

energy density supercapacitors in particular due to their extended operating potential window as high as 1.7 V in aqueous medium.

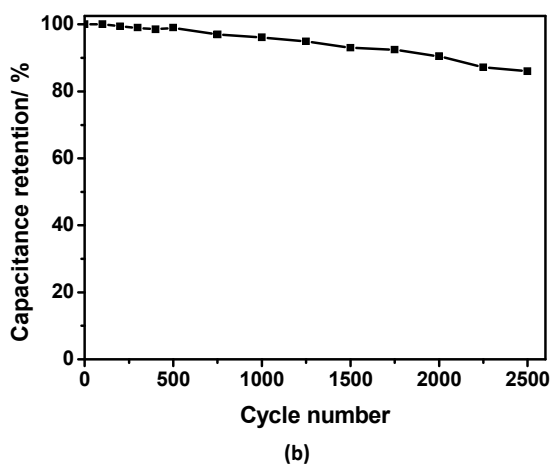
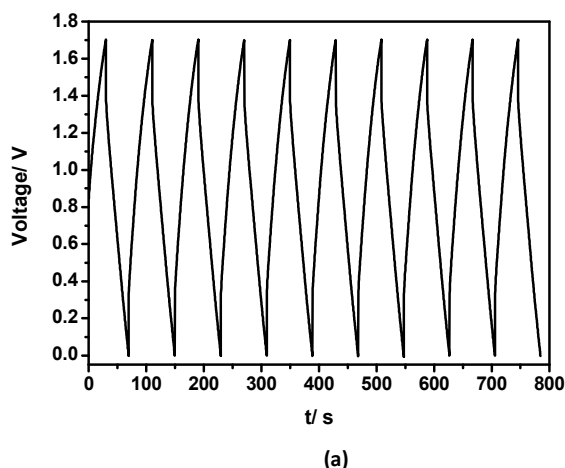


Figure 11. Charge-discharge curves for NiO_x/CNF-CNF cell obtained at 1 A g⁻¹ (a). Variation of specific capacitance as a function of cycle numbers (b).

4. Conclusions

The production of a NiO_x/CNF composite as supercapacitor electrode has been demonstrated by using a one-step anodic electrodeposition process. The use of Na₂SO₄ as electrolyte, a neutral and environmentally friendly solution, shows that the composite electrode can operate in a very broad potential window as high as 2.2 V. The resulting supercapacitor electrode delivers a

specific capacitance of 150 F g⁻¹ at 1 A g⁻¹ considering the total mass of the electrode (deposit plus substrate) with 88.5% capacitance retention after 2500 cycles. In addition, it has been shown the simultaneous formation of Ni²⁺ and Ni³⁺ species, confirmed by XPS, during the electrodeposition process which might lead to the existence of pseudocapacitance as evidenced in MnO₂ and RuO₂ materials.

The best performance composite electrode, prepared at 2 mA cm⁻², was connected to pure CNF in order to simulate an asymmetric EC; the proposed cell displayed energy and power density values of 29 Wh kg⁻¹ and 4 kW kg⁻¹, respectively. Moreover, the cell retains 85 % of its capacitance after 2500 cycles. These results suggest the potential application of the prepared composites in high energy density electrochemical capacitors.

Acknowledgments

The authors would like to acknowledge FCT for financial support under the project M-ERA.NET/0002/2012, COST Action MP 1004 "Hybrid Energy Storage Devices and Systems for Mobile and Stationary Applications", and PEst-OE/QUI/UI0100/2013.

References

- 1 J. R. Miller, *Electrochim. Acta*, 2006, **52**, 1703-1708.
- 2 J. Yan, Q. Wang, T. Wei and Z. Fan, *Adv. Energy Mater.*, 2014, **4**, 1300816 (1-43).
- 3 B. Dunn, H. Kamath and J. -M. Tarascon, *Science*, 2011, **334**, 928-935.
- 4 M. Zhi, C. Xiang, J. Li, M. Li and N. Wu, *Nanoscale*, 2013, **5**, 72-88.
- 5 D. -D. Zhao, S. -J. Bao, W. -J. Zhou and H. -L. Li, *Electrochem. Commun.*, 2007, **9**, 869-874.
- 6 M. -S. Wu and K. -C. Huang, *Chem. Commun.*, 2011, **47**, 12122-12124.
- 7 Y. Tang, Y. Liu, S. Yu, Y. Zhao, S. Mu and F. Gao, *Electrochim. Acta*, 2014, **123**, 158-166.
- 8 T. Brousse, D. Bélanger and J. W. Long, *J. Electrochem. Soc.*, 2015, **162**, A5185-A5189.
- 9 J. W. Kim, V. Augustyn and B. Dunn, *Adv. Energy Mater.*, 2012, **2**, 141-148.

ARTICLE

Journal Name

- 10 D. Rochefort and A. -L. Pont, *Electrochem. Commun.*, 2006, **8**, 1539-1543.
- 11 R. Della Noce, S. Eugénio, T. M. Silva, M. J. Carmezim and M. F. Montemor, *J. Power Sources*, 2015, **288**, 234-242.
- 12 M. Chigane and M. Ishikawa, *J. Chem. Soc. Faraday Trans.*, 1992, **88**, 2203-2205.
- 13 M. -S. Wu, Y. -A. Huang, J. -J. Jow, W. -D. Yang, C. -Y Hsieh and H. -M. Tsai, *Int. J. Hydrogen Energy*, 2008, **33**, 2921-2926.
- 14 A. C. Sonavane, A. I. Inamdar, P. S. Shinde, H. P. Deshmukh, R. S. Patil and P. S. Patil, *J. Alloys Compd.*, 2010, **489**, 667-673.
- 15 G. H. A. Therese and P. V. Kamath, *Chem. Mater.* 2000, **12**, 1195-1204.
- 16 G. W. D. Briggs and M. Fleischmann, *Trans. Faraday Soc.*, 1966, **62**, 3217-3228.
- 17 W. Eysel, H.H. Hofer, K.L. Keester, and T. Hahn, *Acta Crystallographica, Section B*, 1985, **41**, 5-11.
- 18 S. Sasaki, K. Fujino, and Y. Takeuchi. *Proc. Jpn. Acad., Ser. B*, 1979, **55**, 43-48.
- 19 P. A. Thiel and T. E. Madey, *Surf. Sci. Rep.*, 1987, **7**, 211-385.
- 20 R. P. Silva, S. Eugénio, R. Duarte, T. M. Silva, M. J. Carmezim and M. F. Montemor, *Electrochim. Acta*, 2015, **167**, 13-19.
- 21 C. E. Dubé, B. Workie, S. P. Kounaves, A. Robbat Jr, M. L. Aksu and G. Davies, *J. Electrochem. Soc.*, 1995, **142**, 3357-3365.
- 22 A. Mansour and C. Melendres, *Surf. Sci. Spectra*, 1994, **3**, 271-278.
- 23 X. Qin, X. Li, L. Yang, Z. Wang, B. Zheng, H. Yuan and D. Xiao, *J. Alloys Compd.*, 2014, **610**, 549-554.
- 24 L. Gu, Y. Wang, R. Lu, L. Guan, X. Peng and J. Sha, *J. Mater. Chem. A*, 2014, **2**, 7161-7164.
- 25 C. A. Melendres and A. N. Mansour, *Electrochim. Acta*, 1997, **43**, 631-634.
- 26 M. Balasubramanian, C. A. Melendres and A. N. Mansour, *J. Electrochem. Soc.*, 1999, **146**, 607-614.
- 27 C. -C. Hu and T.-Y. Hsu, *Electrochim. Acta*, 2008, **53**, 2386-2395.
- 28 F. Béguin, K. Kierzek, M. Friebe, A. Jankowska, J. Machnikowski, K. Jurewicz and E. Frackowiak, *Electrochim. Acta*, 2006, **51**, 2161-2167.
- 29 W. Jiang, S. Zhai, L. Wei, Y. Yuan, D. Yu, L. Wang, J. Wei and Y. Chen, *Nanotechnology*, 2015, **26**, 314003 (1-10).
- 30 Y. Tan, W. Zhang, Y. Gao, J. Wu and B. Tang, *J. Mater. Sci.*, 2015, **50**, 4622-4628.
- 31 G. A. Lange, S. Eugénio, R. G. Duarte, T. M. Silva, M. J. Carmezim and M. F. Montemor, *J. Electroanal. Chem.*, 2015, **737**, 85-92.
- 32 S. Cheng, L. Yang, Y. Liu, W. Lin, L. Huang, D. Chen, C. P. Wong and M. Liu, *J. Mater. Chem. A*, 2013, **1**, 7709-7716.
- 33 M. Toupin, T. Brousse and D. Bélanger, *Chem. Mater.*, 2002, **14**, 3946-3952.
- 34 M. Toupin, T. Brousse and D. Bélanger, *Chem. Mater.*, 2004, **16**, 3184-3190.
- 35 W. Sugimoto, K. Yokoshima, Y. Murakami and Y. Takasu, *Electrochim. Acta*, 2006, **52**, 1742-1748.
- 36 Y. Zhang, C. Zhang, G. Huang, B. Xing and Y. Duan, *Electrochim. Acta*, 2015, **166**, 107-116.
- 37 D. C. Silverman, *Corrosion*, 1981, **37**, 546-548.

Anodic electrodeposition of NiO_x ($\text{NiO} + \text{NiOOH}$) onto carbon nanofoam forming a supercapacitor electrode. The resulting composite electrode operates at 2.2 V in Na_2SO_4 aqueous medium.

